Robotica (2015) volume 33, pp. 1536–1550. © Cambridge University Press 2014
doi:10.1017/S0263574714000137

Collision analysis and safety evaluation using a collision model for the frontal robot–human impact

Jung-Jun Park†, Jae-Bok Song‡* and Sami Haddadin§

†*Manufacturing Center, Samsung Electronics, Seoul, Republic of Korea*
‡*School of Mechanical Engineering, Korea University, Seoul, Republic of Korea*
§*Institute of Automatic Control, Leibniz University Hanover (LUH), Germany*

(Accepted January 8, 2013. First published online: April 15, 2014)

SUMMARY
The safety analysis of human–robot collisions has recently drawn significant attention, as robots are increasingly used in human environments. In order to understand the potential injury a robot could cause in case of an impact, such incidents should be evaluated before designing a robot arm based on biomechanical safety criteria. In recent literature, such incidents have been investigated mostly by experimental crash-testing. However, experimental methods are expensive, and the design parameters of the robot arm are difficult to change instantly. In order to solve this issue, we propose a novel robot-human collision model consisting of a 6-degree-of-freedom mass-spring-damper system for impact analysis. Since the proposed robot-human consists of a head, neck, chest, and torso, the relative motion among these body parts can be analyzed. In this study, collision analysis of impacts to the head, neck, and chest at various collision speeds are conducted using the proposed collision model. Then, the degree of injury is estimated by using various biomechanical severity indices. The reliability of the proposed collision model is verified by comparing the obtained simulation results with experimental results from literature. Furthermore, the basic requirements for the design of safer robots are determined.

KEYWORDS: Physical human–robot interaction; Collision analysis and model; Safe robots; Human injury analysis.

1. Introduction and Background

SINCE the introduction of service robots in human environments, safety issues related to physical human–robot interaction have become increasingly important. Collision analysis and safety evaluations of physical interactions between humans and robots have been investigated extensively.[1–10] To quantify the potential danger of robot arms for blunt contact, real impact tests have been conducted using a Hybrid III dummy. The intrinsic properties of the collisions between humans and robot arms were studied by applying various biomechanical severity indices.[1,2] For safety evaluation, several collision studies used reduced collision models composed of a human head mass and a robot mass, whose motions were converted into translations.[3–5] Recently, impact simulations with robot arms used the head and chest of a clamped human dummy.[6] In addition to the direct impact consequences at the primary location of impact, neck bending during a head impact posed only very limited potential of injury for collision speeds under 2 m/s.[1,2]

However, in order to support these findings and generalize them to any kind of robot, the bonding effects between the head, neck, and torso should be simulated but not using only simplified models of body parts. Furthermore, there is no consensus on the sufficient set of safety criteria or on the standard experimental setup for the simulation of safety critical situations in physical human–robot interaction. An obvious problem with safety evaluation based on real crash-tests is the substantial amount of time and expense needed to construct experimental setups, conduct experiments, and

* Corresponding author. E-mail: jbsong@korea.ac.kr

analyze data. Furthermore, to evaluate the collision safety of a robot arm in the design stage, realistic collision experiments should be conducted, although this is not easy.

To generalize the findings in the literature to be applicable to any robot-human impact cases, we propose a collision model composed of multiple body parts and a robot arm, which will give reasonably accurate simulation results. The proposed collision model is verified with the experimental crash-test results obtained from.[1,2] This model is considered a simple yet sufficient model for fast intrinsic safety evaluation during the robot design stage. The proposed human frontal model consists of a head, neck, chest complex, and a torso, so it can be used for impact analysis of various collision situations. Head, neck, and chest injuries are estimated by calculating a set of severity indices, which were used in the robotics literature. The robot model can be used for a general type of robot. Various dynamic collisions were simulated using the proposed collision model, and the results were evaluated according to injury indices for the head, neck, and chest. Moreover, important robot design parameters are determined according to the presented collision analysis.

In contrast to existing work, the present study introduces a collision model with multiple human body parts. The model can be used to evaluate collision safety according to various injury criteria of different body parts. Therefore, a full analysis can be conducted without the expensive, real collision tests. Of course, the real robot design needs to be analyzed experimentally; however, the proposed methodology allows the use of simulation insights early in the design stage, making it possible to design safer robot arms and to determine safe operating conditions before real testing. This shortens development cycles significantly.

This paper is organized as follows. Injury criteria for physical human–robot interaction mainly adopted from biomechanics are discussed in Section 2. Section 3 describes our collision conditions. Various impact evaluations and the identification of important robot design parameters for design of safer arms are provided in Section 4. Finally, Section 5 concludes the paper.

2. Injury Criteria for Physical Human–Robot Interaction

Several types of safety criteria for physical human–robot interaction have been suggested up to now,[7,8] which seem to be rather conservative compared to that reported in existing literature. To resolve the imposed limitations of these safety criteria, the injury assessment from automobile crash-testing, which evaluated the collision characteristics between humans and robots, was applied to human–robot interaction.[5]

Contacts upon human–robot impacts can generally be divided into unconstrained impacts, constrained impacts, and partially constrained impacts, which include both blunt impacts and sharp-edge impacts. Of course, sharp-edge impacts can cause severe injury to a human. However, in this paper we focus on blunt impact to a human as a beginning stage of collision analysis. Next, we briefly review head, neck, and chest injury criteria for blunt impact analysis, which are widely used in the literature on crash testing.

2.1. Head injury

The head is one of the most critical body parts to be protected from impact trauma, as the consequent injury can be devastating. The brain may be injured by two major types of processes: first, excessive acceleration of the head and second, a fracture of a cranial bone by direct impact to the head. In order to cover the wide range of blunt head injuries, various injury criteria for the head were developed. Among several injury criteria used in automobile crash-testing, the Head Injury Criterion (HIC) is most widely used in the robotics community. HIC36 is defined as

$$\mathrm{HIC}_{36\mathrm{ms}} = \max\left\{(t_2 - t_1)\left[\frac{1}{t_2 - t_1}\int_{t_1}^{t_2} \|\ddot{x}_H\| dt\right]^{2.5}\right\} \quad \text{for} \quad t_2 - t_1 \leq 36\ \mathrm{ms}, \tag{1}$$

where $\|\ddot{x}_H\|$ is the resulting head acceleration expressed in g ($= 9.8\ \mathrm{m/s^2}$) during the time interval (t_2 - t_1). HIC can then be converted into an injury scale as the Abbreviated Injury Scale.[11] An HIC value below 650, for instance, represents a probability of serious injury (AIS $\geq$3) being less than 5%.

Table I lists fracture tolerances of cranial and facial bones including the impactor sizes used in their respective collision experiments. An impact test with differently sized impactors verified that

https://doi.org/10.1017/S0263574714000137 Published online by Cambridge University Press

Table I. Facial impact tolerances of human cadaver heads.

Cranial bone	Fracture force	Impactor size
Frontal bone[21]	4.0 kN	ϕ 0.02 m
Temporoparietal bone[22]	3.12 kN	ϕ 0.029 m
Maxilla bone[23]	0.66 kN	ϕ 0.029 m
Nasal bone[24]	0.34 kN	ϕ 0.023 m

Table II. Injury tolerances of the human neck.

Indirect impact	Injury tolerance
Shear[18]	3.1 kN@0 ms, 1.5 kN@30 ms, 1.1 kN@45 ms
Tension[18]	3.3 kN@0 ms, 2.9 kN@35ms, 1.1 kN@60 ms
Compression[18]	4 kN @ 0 ms, 1.1 kN @ 30ms
Extension[19]	57 Nm
Flexion[19]	190 Nm
Direct impact	Injury tolerance
Thyroid and cricoids[20]	0.337–0.810 kN

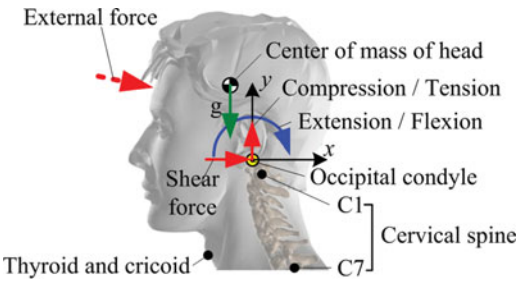

Fig. 1. Descriptions of head loading and anatomy of neck.

both the maximum pressure[12] and the maximum contact force[13] acting on the bone are related to bone fracture. Thus, we discuss the fracture force of each part with the information on the impactor size to consider simultaneously both the force and the pressure in this study.

2.2. *Neck injury*

Neck injuries can occur by direct or indirect impacting. An indirect impact denotes a collision force or acceleration acting on the head that affects the spinal column of the neck. In automobile collisions, neck injuries often occur as a result of bending due to inertial loading of the head.[18,19] When the body is violently accelerated or decelerated, potentially injurious neck loads and large deflections are generated by the inertia and motion of the head. For instance, if an external force is applied to the human head in the x-y plane as shown in Fig. 1, an extension/flexion moment, a compression/tension force in the direction of the y-axis, and a shear force in the direction of the x-axis occur at the occipital condyle.

Table II lists the injury tolerance values of the neck according to the neck loading type. The injury tolerances due to shear force, tension force, and compression force are given as time-dependent curves. As the impact duration increases, the tolerance values of the neck decreases; this means the neck injury risk increases with impact duration.

Upon direct frontal impact to the neck, in the anterior portion of the neck, two stiff tissues - thyroid cartilage and cricoid cartilage - may be hit. These stiff tissues are found at the upper end of the airway passage in the neck, and are delicate and vital because their collapse may obstruct airflow (the tissue itself is non-vital). When an impact is applied to the thyroid and cricoid simultaneously, the dynamic fracture load is about 0.34 kN.

https://doi.org/10.1017/S0263574714000137 Published online by Cambridge University Press

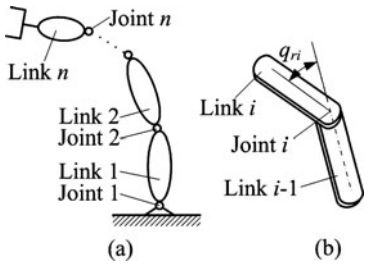

Fig. 2. Robot arm model for collision analysis. (a) n-link robot model, and (b) connection between link i and link $i-1$.

2.3. Chest injury

The chest contains internal organs such as the heart and lungs, which are protected and supported by the sternum, rib cage, and spine. The maximum tolerable contact force to the chest with respect to pain lies in the range from 1.15 kN to 1.7 kN.[21] The compression criterion (CC)[22] and the viscous criterion (VC)[23] were found to overcome this limitation. For the CC, the thoracic deflection should be less than 22 mm. The VC, also known as the soft tissue criterion, can be expressed as

$$\mathrm{VC} = c_c \, \|\Delta \dot{x}_c\|_2 \, \frac{\|\Delta x_c\|_2}{l_c} \leq 0.5 \ \mathrm{m/s}, \tag{2}$$

where $\Delta \dot{x}_c$ is the compression velocity of the chest and Δx_c is the thoracic deflection. The scaling factor c_c and the initial torso thickness l_c depend on the dummy used.

3. Collision Model for Human and Robot

3.1. Modeling of human and robot

The consideration of collision safety in the design stage of a robot is highly desirable because the time and cost involved in real collision tests can be significantly be reduced or at some point even be eliminated. As previously mentioned, isolated collision models for each body part have been typically considered up to now. In this study, we propose a more complex human model consisting of a head, neck, chest, and torso. The robot is modeled as an articulated chain of rigid bodies that interact with the environment via contact forces that are projected via their respective Jacobian into the joints. Generally, a robot manipulator consisting of n-links is considered, see Fig. 2. The position of joint i is uniquely denoted by θ_{ri}, so we do not consider elastic manipulators. During impact this n-link manipulator can be interpreted as a one-dimensional reflected mass model,[24] which value depends on the relevant Cartesian translational direction of the reflected robot inertia tensor $M_c \in \Re_{3\times 3}$ at the robot collision location. Generally, the joint space mass matrix of a robot can be transformed into its Cartesian equivalence via equivalence of kinetic energy. The reflected Cartesian mass matrix is defined as

$$M_c = \left(J_{r,v}(\theta) M_r(\theta)^{-1} J_{r,v}(\theta)^T \right)^{-1}, \tag{3}$$

where θ is the link angle of the robot, $M_r(\theta) \in \Re_{n\times n}$ is the link mass matrix, and $J_{r,v}(\theta) \in \Re_{3\times n}$ is the manipulator Jacobian matrix associated with the linear velocity at the end-point of the robot arm.

In this paper, we consider the seated human model, consisting of a head, neck, chest, and torso, modeled as a 5-DOF mass-spring-damper system rotating about the z-axis, as shown in Fig. 3(b). The head, modeled as link 3, rotates around the occipital condyle (O.C.) where the base of the skull is connected to the C1 vertebra. The cervical spine, which consists of seven vertebrae from C1 to C7 as shown in Fig. 1, is the most important part of the neck. Therefore, the neck is modeled as link 2, which is able to rotate around the C7 vertebra. Rotary springs and dampers are inserted at the occipital condyle and the C7 vertebra of the neck model. Since we assume a human to sit on a chair without a backrest, the torso was assumed to rotate only around the hip joint (H-point). The parameters of

https://doi.org/10.1017/S0263574714000137 Published online by Cambridge University Press

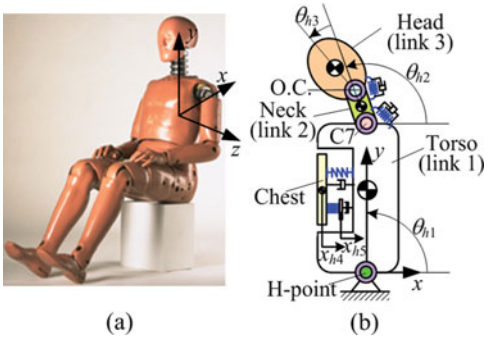

Fig. 3. Seated human model for collision analysis. (a) seated Hybrid-III dummy, and (b) side view of 5-DOF human model.

the human model were set to the same values as those of the seated Hybrid III 50th percentile male dummy, which is the most widely used dummy for a crash test.

For the head, neck and torso, the following numerical values hold: $m_{h3} = 4.5$ kg, $m_{h2} = 1.4$ kg, $m_{h1} = 40.2$ kg, $I_{h3} = 0.024$ kgm^2, $I_{h2} = 0.003$ kgm^2, $l_{hc3} = 0.0508$ m, $l_{h2} = 0.124$ m, and $l_{h1} = 0.528$ m,[25] where m_{hi} and I_{hi} are the mass and the moment of inertia of link i, respectively and the link lengths, and the lengths of the center of mass of the links, are represented by l_{hi} and l_{hci}, respectively. Since neck stiffness varies depending on the direction of rotation of the head (i.e., extension or flexion), the stiffness and damping of a dummy neck according to the angular velocities of the head and the neck are described by

$$k_{3n} = \begin{cases} 4.51 & \text{Nm/}^\circ, \quad \dot{\theta}_3 \geq 0 \\ 1.89 & \text{Nm/}^\circ, \quad \dot{\theta}_3 < 0 \end{cases} \tag{4a}$$

$$k_{2n} = \begin{cases} 4.51 & \text{Nm/}^\circ, \quad \dot{\theta}_2 \geq 0 \\ 1.89 & \text{Nm/}^\circ, \quad \dot{\theta}_2 < 0 \end{cases} \tag{4b}$$

where the neck stiffness for extension and flexion are the values used for a Hybrid III's neck.[25] The damping coefficient is obtained from $c_n = 2\zeta_n\sqrt{I_h k_n}$. Therefore, when the damping ratio of a neck ζ_n is set to 0.2, the resulting damping values are 0.22 Nm.s/$^\circ$ and 0.19 Nm.s/$^\circ$ according to the direction of rotation, respectively.

For the chest model, a lumped-mass model developed by Lobdell[26] is used in this paper. To obtain the definite form of the inertia matrix, Lobdell's chest model is modified according to Fig. 3(b). The sternum mass m_{h4} is connected to the torso mass m_{h1} by a parallel Voigt element (k_r, c_b) and a Maxwell element (k_{ve}, c_{ve}). For the Voigt element, the spring k_r represents the elasticity of the rib cage and the directly coupled viscera, and the damper c_b represents the air in the lungs and blood in the vessels. The Maxwell element represents viscoelastic tissues such as the thoracic muscle tissue. A small dummy mass (m_{h5}) was added between the spring and the damper of the Maxwell element to obtain the definite form of the inertia matrix. The viscoelastic components k_{ve} and c_{ve} were set to 13.12 kN/m and 175 Ns/m, respectively. Because the parameters of the Voigt element vary depending on the sternal deflection, the stiffness k_r and damping value c_b are expressed as

$$k_r = \begin{cases} 26.25 & \text{kN/m}, \quad x_{h5} - x_{h4} < 38\text{mm} \\ 78.75 & \text{kN/m}, \quad x_{h5} - x_{h4} \geq 38\text{mm} \end{cases} \tag{5a}$$

$$c_b = \begin{cases} 525 & \text{Ns/m}, \quad \dot{x}_{h5} \geq \dot{x}_{h4} \\ 1225 & \text{Ns/m}, \quad \dot{x}_{h5} < \dot{x}_{h4} \end{cases} \tag{5b}$$

where all parameters for the chest are taken from Ref. 26.

The contact force relationship between the human body and the robot arm is modeled by a simple spring element, which represents the contact elasticity of the respectively touched body parts. In the following section, we introduce the contact force relationship according to the contacting part of

https://doi.org/10.1017/S0263574714000137 Published online by Cambridge University Press

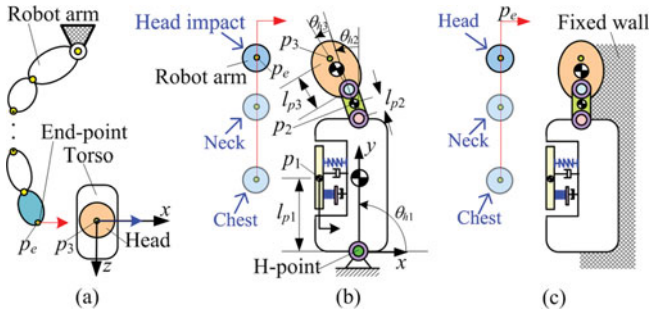

Fig. 4. (a) Top view, and (b) Side view of impact to unconstrained human, and (c) constrained human.

the human body. The stiffness of the spring element is obtained by considering existing data from collision experiments in the literature.

3.2. Equation of motion of collision model

In this section, we derive the dynamic equations of motion for the proposed collision model. A Lagrangian formulation is used to develop the equations of motion. For a general mechanical system consisting of a multi DOF mass - spring - damper system, the dynamic differential equation of motion can be obtained by

$$\begin{bmatrix} f_{r,in} + f_{r,ex} \\ \tau_{h,ex} \end{bmatrix} = \begin{bmatrix} M_c & 0 \\ 0 & M_h \end{bmatrix} \begin{bmatrix} \ddot{x}_r \\ \ddot{\theta}_h \end{bmatrix} + \begin{bmatrix} 0 \\ C_h \end{bmatrix} + \begin{bmatrix} 0 \\ K_h \end{bmatrix} + \begin{bmatrix} 0 \\ D_h \end{bmatrix} + \begin{bmatrix} 0 \\ G_h \end{bmatrix}, \tag{6}$$

where M_h, C_h, K_h, G_h, D_h and $\tau_{h,ex}$ are the inertia matrix, centrifugal and Coriolis vector, stiffness vector, gravity vector, damping vector, and external torque vector of the human model, respectively. Moreover, M_c, x_r, θ_h, $f_{r,in}$ and $f_{r,ex}$ are the reflected mass of the robot, the displacement vector of the robot's reflected mass model, the angular displacement vector of the human model, the input force generated by the input torque of each robot joint and the external force acting on the end-point of the robot, respectively.

Figure 4 depicts the robot model and human model according to the contact position of the human body. We assume that the robot end-point only moves in the direction of the x-axis[(1)]. The position vectors of the end-point of the robot arm p_e and the contact points at the human p_i are obtained from forward kinematics.

As mentioned, the contact force due to impact in multi-body systems can be described by

$$|F_c| = \begin{cases} k_c & \delta, \delta \geq 0 \\ 0, & \delta < 0 \end{cases} \tag{7}$$

where k_c is the stiffness constant between the body part and the impactor, and δ is the relative penetration depth, which is given as $\delta = R_e + R_i - |p_i - p_e|$. R_e and R_i are the radii of the end-effector and the human body part, respectively.

For the collision force between the robot arm and each body part, the stiffness constants for a collision with the frontal bone and nasal bone of the head, with the larynx and with the sternum of the chest are set to 1.0×10^6 N/m,[14] 3.8×10^4 N/m,[27] 2.2×10^4 N/m,[20] and 2.8×10^5 N/m,[26] respectively. These values can be obtained from the slope of the force/displacement curves from each reference. These collision conditions are more conservative because the impactor sizes used for

[(1)] In many experiments using cadavers, the impactor collided with a human body part in the vertical direction. Therefore, in this paper, to compare the proposed model with experimental results according to the same collision condition, we considered only the frontal robot-human impact in the direction of x-axis.

https://doi.org/10.1017/S0263574714000137 Published online by Cambridge University Press

collision experiments listed in Table I are very small for the blunt impact. The contact force vector can be obtained by

$$F_c = |F_c| \frac{p_i - p_e}{|p_i - p_e|}. \tag{8}$$

3.2.1. Impact to the human head. First, consider a collision with the human head, see Fig. 4. The external force vector of the robot and the external torque vector of the human for the head impact can be expressed as

$$f_{r,ex} = -F_c \tag{9.a}$$

$$\tau_{h,ex} = J_{h,v}^T F_c, \tag{9.b}$$

where F_c is the contact force between the head and the robot arm, and $J_{h,v}$ represents the Jacobian matrix associated with the linear velocity at the contact point of the human head. Note that the external torque vector of the human model changes depending on the contacting part of the human body.

The input force vector at the end-point of the n-link manipulator can be obtained by

$$f_{r,in} = \begin{cases} (J_{r,v}^T)^{-1} \tau_{r,in}, & n = 3 \\ J_{r,v}(J_{r,v}^T J_{r,v})^{-1} \tau_{r,in}, & n > 3 \end{cases} \tag{10}$$

where $\tau_{r,in} \in \Re_{n\times 1}$ is the input torque applied to joint i, and $J_{r,v}$ represents the Jacobian matrix associated with the linear velocity at the end point of the robot. The joint torque is defined via a PD-control law $\tau_{r,in} = k_{pi}(\theta_{di} - \theta_{ri}) - k_{vi}\dot{\theta}_{ri}$ where θ_{di} is the desired angle of joint i, and k_{pi} and k_{vi} are the proportional and derivative gains of joint i for position control of the robot arm. In this study, the selection of the feedback controller of the robot arm did not affect the analysis results.

3.2.2. Impact to neck of human. Next, consider an impact acting directly on the neck of a human, as shown in Fig. 4. Since only the contact position of the neck changes, M_h, K_h, C_h, G_h, and D_h remain unchanged. The external torque vector can now be expressed as

$$\tau_{h,ex} = \begin{bmatrix} -F_{cx}(l_{h1}\sin\theta_{h1} + l_{c2}\sin\theta_{h12}) + F_{cy}(l_{h1}\cos\theta_{h1} + l_{c2}\cos\theta_{h12}) \\ -F_{cx} l_{c2}\sin\theta_{h12} + F_{cy} l_{c2}\cos\theta_{h12} \\ 0 \\ 0 \\ 0 \end{bmatrix}, \tag{11}$$

where the link lengths of the human model are represented by l_{hi}, and θ_{hi} and θ_{h12} represent θ_{h1} and $\theta_{h1}+\theta_{h2}$, respectively.

3.2.3. Impact to the human chest. For the case of a robot arm directly colliding with the human chest, the collision model is shown in Fig. 4. Since only the generalized force term of eq. (6) is changed, the matrices M_h, K_h, C_h, G_h, and D_h (except τ) are the same as those of the two previous cases. The external torque vector is given by

$$\tau_{h,ex} = \begin{bmatrix} -F_{cx} l_{c1}\sin\theta_{h1} + F_{cy} l_{c1}\cos\theta_{h1} \\ 0 \\ 0 \\ |F_c| \\ 0 \end{bmatrix}. \tag{12}$$

https://doi.org/10.1017/S0263574714000137 Published online by Cambridge University Press

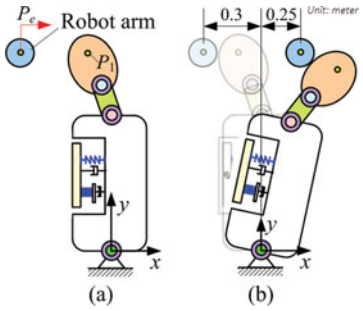

Fig. 5. Configurations of 1-link manipulator. (a) Before the collision, and (b) at the collision instant and afterwards.

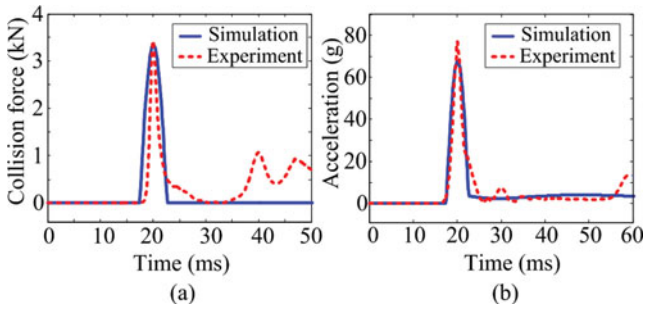

Fig. 6. Comparison between simulation and experimental results. (a) Collision force to head, and (b) head acceleration for collision velocity of 2.0 m/s and reflected inertia of 67 kg.

4. Impact Simulation, Safety Evaluation, and Safe Arm Design

4.1. Collision simulation

The collision analysis of an impact to the frontal bone, nasal bone, neck, and chest of an unconstrained and constrained human is carried out. For this, we used KUKA KR 6, which is a typical standard medium-scale industrial manipulator. The reflected mass perceived at the end-point of KR6 along the x-axis is 67 kg[5] for the stretched-out impact configuration. The lengths from the occipital condyle to the contact point of the frontal bone and the nose l_{c1} are set to 0.12 m and 0.09 m, respectively. The contact position of the neck from the C7 vertebra l_{c2} is chosen to be 0.07 m and the distance between the contact position of the chest and the H-point l_{c1} is 0.36 m.

Since eq. (6) is a coupled second-order nonlinear differential equation for the displacement vector θ_h and x_r, it has to be solved numerically. In case of the unconstrained human model, the initial position of the reflected mass of the robot arm is –0.75 m in the x-axis direction and this mass is forced to collide with the human head at –0.3 m with a predefined velocity. Then, the robot stops at 0.25 m in the x-axis direction, see Fig. 6. Note that no safe reaction control is used for the unconstrained impact.

On the other hand, in case of the impact to a constrained human, the human body parts (head, neck and torso, except chest) are fully constrained, as shown in Fig. 4(c). The angular displacements of the head, the neck, and the torso are set to fixed values ($\theta_{h3} = \theta_{h2} = 0^\circ$ and $\theta_{h1} = 90^\circ$). Therefore, the collision with the constrained head and neck can be regarded as an impact to a fixed wall having infinite mass. We utilized the robot impact reaction strategy stop category 0,[6] in which the motor drives of the robot arm are immediately switched off and the brakes engage at the same time as soon as collision is detected.

4.2. Verification of proposed collision model against experimental results

To verify the reliability of the proposed collision model, the simulation results are compared with experimental results from Ref. 1. In this work, various experiments with blunt impacts were performed using the industrial robots KUKA KR6, KR500, and LWRIII for blunt impacts to the head and chest of a frontal Hybrid III crash test dummy.

https://doi.org/10.1017/S0263574714000137 Published online by Cambridge University Press

Table III. Comparison between simulation and experimental results unconstrained head impacts.

v_{end} (m/s)	$F_{frontal}$ (kN) Sim./Exp.	HIC Sim./Exp.	a_{max} (g) Sim./Exp.	F_{shear} (kN) Sim./Exp.	$M_{flexion}$ (Nm) Sim./Exp.
0.2	0.33/0.12	0.2/0.03	6.7/1.6	0.06/0.09	2.8/1.9
0.7	1.17/0.78	4.7/2.2	23.6/13.4	0.21/0.18	9.7/7.8
1.0	1.67/1.31	11.2/6.7	33.7/23.5	0.30/0.32	13.8/13.7
1.3	2.17/1.88	22.1/16.7	43.9/37.8	0.39/0.47	17.9/25.3
1.5	2.51/2.21	31.2/25.5	50.6/45.6	0.45/0.48	20.6/29.0
2.0	3.34/3.43	64.2/64.4	67.5/77.2	0.59/0.71	27.2/43.0

Table IV. Sample conditions of real facial impact tests[36].

No. of Exp.	Impactor Mass (kg)	Collision Speed (m/s)	Fracture parts
20	32	4.75	Nasal bone
25	32	4.47	Nasal bone
29	32	6.33	Nasal, maxillary bone
34	32	7.14	Nasal, maxilla, zygomatic bone
42	64	3.44	Nasal bone

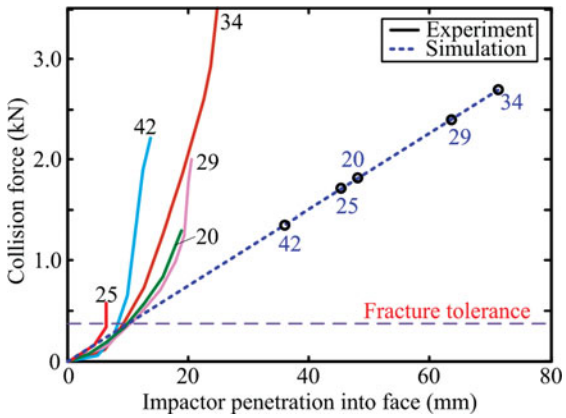

Fig. 7. Comparison of simulation and experimental results for nose impact with reflected inertia described in Table IV.

First, KR6 impacts to the forehead of the Hybrid III dummy are compared. As shown in Table III, these simulation results, including the maximum collision force to the head, HIC, maximum resultant head acceleration, neck force, and neck moment show reasonably good agreement with the experimental results from real collisions. Furthermore, as shown in Fig. 6, the shapes of the collision force and head acceleration curves in the simulation results are very similar to those of the experimental results.

Second, to evaluate the validity of the nose impact of the proposed model, the simulation results are compared with the experimental results using cadavers[27] because the Hybrid-III dummy does not guarantee the biofidelity for nasal bone impacts. Figure 7 shows the relationship between the impactor penetration depth into the face and the collision force of experimental and simulation results according to experimental conditions in Table IV. When the collision force is below the fracture tolerance of the nasal bone, the stiffness between experiment and simulation is similar. In real facial impact tests, the fracture of the nasal bone occurs relatively easily, but the slope of the curve dramatically increases after the nasal bone fracture incident because one or more of the maxilla, zygoma, sphenoid, and frontal bones sustain the large collision force. Therefore, the proposed collision model for evaluation of the nasal bone fracture is verified.

https://doi.org/10.1017/S0263574714000137 Published online by Cambridge University Press

Table V. Comparison between simulation and experimental results for impact to chest of unconstrained human.

v_{end} (m/s)	F_{chest} (N) Sim./Exp.	CC (mm) Sim./Exp.	VC (m/s) Sim./Exp.	$a_{3ms-chest}$ (g) Sim./ Exp.
0.2	0.15/0.22	4.6/2.7	0.00/0.00	0.17/0.41
0.7	0.48/0.69	14.1/7.6	0.02/0.00	0.66/1.50
1.0	0.68/0.88	19.9/10.6	0.03/0.01	0.95/1.73
1.5	1.02/1.16	29.6/14.0	0.07/0.02	1.45/2.51
2.0	1.36/1.53	39.1/19.1	0.13/0.04	1.94 /3.80
4.2	3.09/3.28	58.7/51.3	0.49/0.41	4.07/8.99

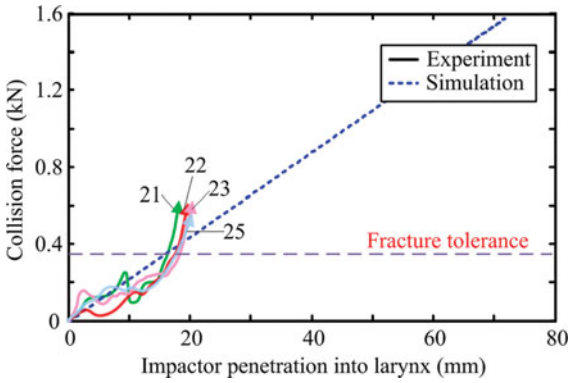

Fig. 8. Comparison between simulation and experimental results for neck impact with reflected inertia of 12 kg.

Third, to evaluate the validity of the proposed model for the evaluation of a direct neck impact, the simulation results are compared with the experimental results[20](2) using large larynges of cadavers in the same manner as the nose impact. The collision speed between the human neck and the robot is set to 3 m/s. The force/penetration slopes obtained from the simulation match those of the cadaver experiments very well before the fractures of the thyroid and cricoids cartilages, see Fig. 8.

Finally, to evaluate the validity of the proposed model for the evaluation of a chest impact, the simulation results are compared to the experimental results of the DLR Crash Report, see Table V. Simulation results according to all criteria related to chest injury, except the chest compression criterion, are very similar to those of the real collision experiments. At low impact velocities in the range from 1.0 m/s to 2.0 m/s, the chest compression values of simulation results are larger than those of experimental results. However, when the collision velocity is 4.2 m/s, both the maximum value and the curve shape of the chest compression and collision force show good agreement with the experimental results, see Fig. 9.

These results may come from the Lobdell chest model, which provides a relatively good collision response of a dummy at a high impact condition such as a car-crash test. Figure 10 shows recommended response guidelines for a dummy design, impact responses of the Hybrid-III dummy, and simulation results of impact response using the proposed collision model.[29] The simulated dummy thorax responses show a good fit with recommended corridors at high collision speed. In this study, we use the Lobdell chest model, because we are not aware of the existence of a more accurate chest model for low collision velocities below 2.0 m/s.

As shown in the preceding comparison of results, the simulation results using the proposed collision model matched the experimental results with sufficient accuracy. This enables us to evaluate the collision safety of a robot arm according to various injury criteria of body parts.

(2) In the paper, compressive strain–load behavior curves were represented, with no notes on the sizes of the larynges used for the experiments. Thus we applied the average size of an adult male larynx (A-P diameter = 36 mm[29]) to obtain the deformation–load curve.

https://doi.org/10.1017/S0263574714000137 Published online by Cambridge University Press

Table VI. EuroNCAP injury severity and corresponding color code.

Color code	Color	Injury potential
Red		Very High
Brown		High
Orange		Medium
Yellow		Low
Green		Very Low

Table VII. Simulation results for collision with frontal bone.

v_{end} (m/s)	Unconstrained						Constrained
	$F_{frontal}$ (kN)	HIC	a_{3ms} (g)	$F_{comp.}$ (kN)	F_{shear} (kN)	$M_{flexion}$ (Nm)	$F_{frontal}$ (kN)
0.5	√ 0.83	2.2	14.8	0.34	0.20	√ 6.9	x 4.63
1.0	√ 1.67	11.9	30.2	0.62	0.30	√ 13.8	x 9.25
1.5	√ 2.51	31.4	45.2	0.90	0.45	√ 20.6	x 13.87
2.0	√ 3.34	65.1	60.2	1.17	0.59	√ 27.2	x 18.50

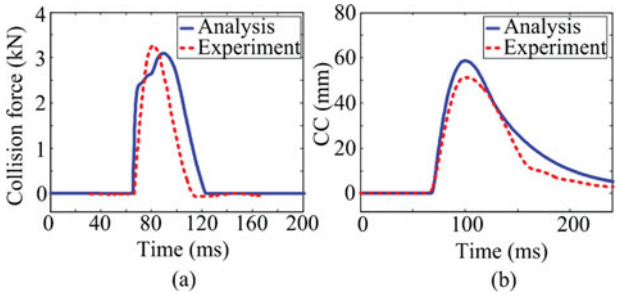

Fig. 9. Comparison between simulation results and experimental results. (a) Chest collision force, and (b) chest compression for a collision velocity of 4.2 m/s and reflected inertia of 4.25 kg.

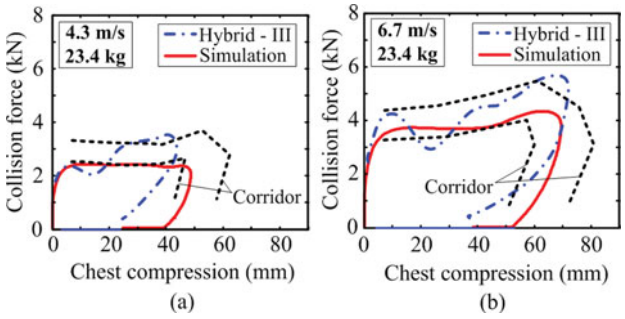

Fig. 10. Blunt frontal thoracic impact response results of Hybrid III dummies and simulation results. Collision speeds are (a) 4.3 m/s, and (b) 6.7 m/s.

4.3. Safety evaluation using the proposed model

4.3.1. Human head impact (Indirect neck impact). In this study, to represent the injury potential of simulation results, a standardized color code in Table VI was utilized (EuroNCAP 2003). This is directly related to the AIS. For indices not included in the EuroNCAP, the injury tolerance values from the literature are evaluated. In Tables VII–X, we used $\surd$ to denote the value which is not critical, $\sim$ value which is in a tolerance band, and x value which is critical according to the injury tolerance.[1]

First, KUKA KR6's collision impact to the frontal bone of the head is simulated for collision speeds between 0.5 m/s and 2.0 m/s. This range corresponds to the normal operating speed of a robot arm in human–robot interaction. Table VII represents the simulation results for the head and neck severity indices introduced in Section 2.

https://doi.org/10.1017/S0263574714000137 Published online by Cambridge University Press

Table VIII. Simulation results for collision with nose.

v_{end} (m/s)	Unconstrained						Constrained
	F_{nose} (kN)	HIC	a_{3ms} (g)	$F_{comp.}$ (kN)	F_{shear} (kN)	$M_{flexion}$ (Nm)	F_{nose} (kN)
0.5	√0.21	0.3	3.5	0.10	0.07	√6.7	x 0.93
1.0	x 0.41	1.5	7.1	0.15	0.11	√13.5	x 2.06
1.5	x 0.61	4.4	10.8	0.20	0.15	√20.0	x 3.18
2.0	x 0.81	9.3	14.5	0.24	0.19	√26.4	x 4.30

Table IX. Simulation results on collision with neck.

v_{end} (m/s)	Unconstrained						Constrained
	F_{neck} (kN)	HIC	a_{3ms} (g)	$F_{tension}$ (kN)	F_{shear} (kN)	$M_{extension}$ (Nm)	F_{neck} (kN)
0.5	√0.29	0.2	2.1	0.05	0.20	6.5	x 0.62
1.0	x 0.56	0.6	4.2	0.06	0.38	12.0	x 1.38
1.5	x 0.83	3.2	6.3	0.06	0.56	17.6	x 2.13
2.0	x 1.09	6.9	8.5	0.06	0.73	23.1	x 2.88

For a collision velocity smaller than 2 m/s, the collision force, the HIC, the maximum average head acceleration for 3 ms, the neck force, and the neck moment do not exceed their respective injury thresholds. The HIC values calculated from Eq. (1) are much lower than 650, which indicates a very low injury possibility. Furthermore, the results indicate that head loading due to impact to the frontal bone at the considered speed does not cause neck injury. This confirms the statements from Ref. 5, where it is argued that a normal range of collision velocities lead to very low intrinsic head injury severity by the HIC and the neck injury criterion. This enables us to limit our analysis to low severity collisions, or other body parts that have not yet been discussed in the robotics literature. In contrast to the unconstrained collision, in case of a constrained impact, a velocity larger than 0.5 m/s is enough to cause fracture of the frontal bone[(3)].

Next, an impact with the human nose is considered. Table VIII represents the simulation results for the injury criteria of the head and neck.

When the robot arm moving at an end-point velocity of 1.0 m/s collides with an unconstrained human, the peak value of the collision force increases to 0.4 kN, which is significantly higher than the fracture tolerance of the nasal bone (0.34 kN). Although there is very low probability of injuries related to head acceleration, neck force, and moment in the normal operation of the robot arm, there is probability of fractures of the nasal bone. As a result, in case of unconstrained impacts, the fracture tolerance of the nasal bone can be regarded as a suitable indicator for a full set of metrics defining the collision safety of robots that work in human environments. Therefore, a robot arm with a reflected inertia of 67 kg (KR6) has to operate below 1.0 m/s

4.3.2. Direct neck impacts. In the collision simulations of direct impact to the neck, the simulation conditions are the same as those for the head impacts. Table IX shows the simulation results for the severity indices related to head and neck injuries including direct neck impacts.

As shown in Table IX, the head acceleration due to a direct impact to the neck leads to very low head injury severity such as HIC and a_{3ms}. This is similar to the case of a direct head collision even for speeds of up to 2 m/s. The shear force, tension force, and extension moment caused by a direct impact to the neck are much lower than injury tolerances.

However, even for impacts to unconstrained humans at these low collision velocities (e.g., 1.0 m/s), the collision force to the neck exceeds the fracture tolerance of the thyroid and cricoid cartilages. Since the obstruction of the airflow due to the collapse of these cartilages is a life-threatening injury,[15] fracture tolerances should also be used to evaluate the collision safety of physical human–robot interaction. Based on the injury tolerance of these cartilages (which is similar to that of the nasal

(3) In real collision experiments, the force profile does not increase further after a bone fracture incident because the stiffness of the human head is dramatically lowered. However, in the simulation, since the contact model in Eq. (6) satisfies Hooke's law which has a constant stiffness, the collision force exceeds the fracture tolerance of the frontal bone with the increase of the penetration depth between the impactor and the frontal bone.

https://doi.org/10.1017/S0263574714000137 Published online by Cambridge University Press

Table X. Simulation results for collision with chest.

	v_{end} (m/s)	F_{chest} (kN)	CC (mm)	VC (m/s)	$a_{3ms\text{-}chest}$ (g)
Unconstrained	0.5	√0.35	10.3	0.01	√0.46
	1.0	√0.68	19.9	0.03	√0.95
	1.5	√1.02	29.6	0.07	√1.45
	2.0	~1.36	39.1	0.13	√1.94
Constrained	v_{end} (m/s)	F_{chest} (kN)	CC (mm)	VC (m/s)	
	0.5	√0.46	16.5	0.01	
	1.0	√1.01	36.2	0.06	
	1.5	x 2.00	50.1	0.13	
	2.0	x 2.99	62.2	0.23	

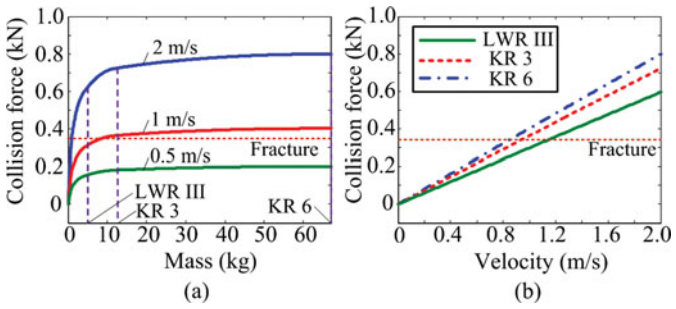

Fig. 11. Simulation results of impact to nasal bone of unconstrained human. (a) collision force versus reflected inertia of robot, and (b) collision force versus collision velocity.

bone), the safe operation condition of a robot arm with a reflected inertia of 67 kg (KR6) requires a maximum velocity smaller than 1.0 m/s in free space.

4.3.3. Human chest impact. Table X summarizes the simulation results for the chest injury criteria. When the robot arm collides with the unconstrained human at 2.0 m/s, the collision force is in the tolerable range of the chest pain, and the compression criterion exceeds 31 mm, which represents medium injury. However, the values of the viscous criterion and the 3 ms criterion are far below their respective injury tolerances, which are 0.2 m/s[30] and 60 g.[23] For a conservative analysis, the chest compression should serve as the appropriate metric, as proposed in ref. [1].

4.4. Design of safer robot arm using collision simulation

Most service robots used in human environments are designed to conduct given tasks such as carrying an object or lifting a heavy load. Therefore, design parameters of an intrinsically safer robot arm should be determined according to given tasks. Typical parameters are the mass moment of inertia, link length of the robot arm, joint stiffness, and operating velocity. In this study, the design parameters of the robot arm were determined based on safety criteria, which are appropriate measures in physical human–robot interaction mentioned in Section 4.3.

Figure 11 shows the collision simulation results for nose impacts as a function of collision velocity and reflected inertia of the robot. If the operating velocity of the robot is set to 1.0 m/s, the reflected inertia of the robot link with a load should be less than 7 kg if nasal bone fracture is to be avoided. Therefore, in the case of the LWR III robot (reflected inertia: 4kg) moving at 1.0 m/s, the desired payload of the robot should be less than 3 kg. For the same operating speed, KR3 (12 kg) and KR6 (67 kg) robots cannot avoid the fracture of the nasal bone, as shown in Fig. 11(a). On the other hand, if the reflected inertia of the robot arm is around 12 kg, which it is for the one of the KR3s, the end-point velocity must not exceed 0.94 m/s, see Fig. 11(b).

In the case of the simulation-based safety estimation, once the collision model is verified by comparing simulation results with experimental results, the collision safety of the robot according to various design parameters can be evaluated by using the collision model in the design stage without

https://doi.org/10.1017/S0263574714000137 Published online by Cambridge University Press

constructing prototypes and conducting experiments repeatedly. Therefore, considerable time and cost can be saved compared to the experiment-based safety estimation.

5. Conclusion

In this study, a novel collision model consisting of a 5 DOF human model and *n*-link robot arm model was proposed. Various verifications and safety investigations were conducted with this model. The proposed collision model can be applied to estimate injury severity due to robot-human collisions and may serve as a valuable tool for design of human-friendly robots. The following conclusions can be drawn:

1) Simulation analysis of human–robot collisions based on biomedical modeling and validation against several experimental data sets was found to be reliable. Therefore, robot collision safety can be evaluated in the robot design stage to save time and cost, which are associated with real collision tests. Passive safety mechanisms as well as active safety oriented control schemes can be investigated with this tool.
2) Appropriate safety criteria for physical human–robot interaction were suggested using the proposed collision analysis approach. The results showed that fractures of the nasal bone, fractures of the thyroid and cricoid cartilage, and chest injury could occur during normal operation of general industrial robot arms, except a light weight robot arm which is below the reflected mass of 4kg.

As our future research work, we will develop the human model that has multi-directional joints to obtain more reliable results of the collision simulation according to various impact conditions.

Acknowledgements

This research was supported by Basic Science Research Program through National Research Foundation of Korea (NRF) (No. 2007-0056094) and by the Ministry of Trade, Industry and Energy under the Industrial Foundation Technology Development Program supervised by the KEIT (No. 10038660). This work has been partially funded by the European Commission's Sixth Framework Program as part of the project SAPHARI under grant no. 287513.

References

1. S. Haddadin, A. Albu-Schaffer, M. Frommberger, J. Rossmann and G. Hirzinger, "The DLR Crash Report: Towards a Standard Crash-Testing Protocol for Robot Safety – Part I: Results," *Proceedings of the IEEE International Conference on Robotics and Automation* (2009) pp. 272–279.
2. S. Haddadin, A. Albu-Schaffer, M. Frommberger, J. Rossmann and G. Hirzinger, "The DLR Crash Report: Towards a Standard Crash-Testing Protocol for Robot Safety – Part II: Discussions," *Proceedings of the IEEE International Conference on Robotics and Automation* (2009) pp. 280–287.
3. J. J. Park, B. S. Kim, J. B. Song and H. S. Kim, "Safe link mechanism based on nonlinear stiffness for collision safety," *Mech. Mach. Theory* **43**(10), 1332–1348 (2008).
4. A. Bicchi and G. Tonietti, "Fast and soft arm tactics: Dealing with the safety-performance tradeoff in robot arms design and control," *IEEE Robot. Autom. Mag.* **11**(2), 22–33 (2004).
5. S. Haddadin, A. Albu-Schäffer and G. Hirzinger, "The Role of the Robot Mass and Velocity in Physical Human–Robot Interaction – Part I: Unconstrained Blunt Impacts," *Proceedings of the IEEE International Conference on Robotics and Automation* (2008) pp. 1331–1338.
6. S. Haddadin, A. Albu-Schaffer and G. Hirzinger, "The Role of the Robot Mass and Velocity in Physical Human–Robot Interaction – Part II: Constrained Blunt Impacts," *Proceedings of the IEEE International Conference on Robotics and Automation* (2008) pp. 1339–1345.
7. ISO-10218, *Robots for Industrial Environments – Safety Requirements – Part 1: Robot* (2006).
8. Y. Yamada, Y. Hirasawa, S.Y. Huang and Y. Umetani, "Fail-Safe Human/Robot Contact in the Safety Space," *IEEE International Workshop on Robot and Human Communication* (1996) pp. 59–64.
9. B. S. Kim, J. B. Song, and J. J. Park, "A Serial-type Dual Actuator Unit with Planetary Gear Train: Basic Design and Applications," *IEEE/ASME Trans. Mechatronics* **15**(1), 108–116 (2010).
10. D. Kulic and E. A. Croft, "Pre collision safety strategies for human robot interaction," *Auton. Robots* **22**(2), 149–164 (2007).
11. AAAM, *The Abbreviated Injury Scale (1990) Revision Update 1998* (Association for the Advancement of Automotive Medicine, Barrington, IL, 1998).
12. A. M. Nahum. "The prediction of Maxillo facial trauma". *Trans Am. Acad. Opth. Otol*. **84**, 932–933 (1976).
13. V. R. Hodgson, "Tolerance of facial bones to impact," *Am. J. Anat.* **120**, 113–122 (1967).

14. D. L. Allsop, C. Y. Warner, M. G. Wille, D. C. Schneider and A. M. Nahum, "Facial Impact Response - A Comparison of the Hybrid III Dummy and Human Cadaver (SAE Paper No.881719)," *Proceedings of the 32th Stapp Car Crash Conference* (1988) pp.781–797.
15. J. Melvin, "Human Tolerance to Impact Conditions as related to Motor Vehicle Design". *SAE J885 APR80.* (1980).
16. D. C. Schneider and A. M. Nahum, "Impact Studied of Facial Bone and Skull," *Proceedings of the 16th Stapp Car Crash Conference*, SAE Paper No. 720965 (1974) 186 pp.
17. J. J. Swearingen, *Tolerances of the Human Face to Crash Impact* (Federal Aviation Agency, Civil Aeromedical Research Institute, Oklahoma City, USA, 1965).
18. H. J. Mertz, *Anthropomorphic test devices. Accidental Injury - Biomechanics and Prevention* Chapter 4 (Springer-Verlag, Berlin, Germany, 1993).
19. H. J. Mertz and L. M. Patrick, "Investigation of the Kinematics and Kinetics of Whiplash," *Proceedings of the 11th Stapp Car Crash Conference*, SAE Paper No. 670919 (1967) pp. 267–317.
20. J. W. Melvin, "Response of Human Larynx to Blunt Loading," *Proceedings of the 17th Stapp Car Crash Conference*, SAE Paper No. 730967. (1973).
21. L. Patrick, "Impact Force Deflection of the Human Thorax," *Proceedings of the 25th Stapp Car Crash Conference*, SAE Paper No. 811014 (1981) pp. 471–496.
22. C. Kroell, D. Scheider and A. "Nahum, Impact Tolerance and Response of the Human Thorax," *Proceedings of 15th Stapp Car Crash Conference*, SAE Paper No.710851 (1971) pp. 84–134.
23. I. Lau, and D. Viano, "Thoracic Impact: A Viscous Tolerance Criterion," *Proceedings of 10th Experimental Safety Vehicle Conference* (1985).
24. O. Khatib, "Inertial properties in robotic manipulation: An object-level framework," *Int. J. Robot. Res.* **14**(1), 19–36 (1995).
25. I. Kaleps and J. Whitestone, "Hybrid III Geometrical and Inertial Properties," *SAE Paper No.880638* (1988).
26. T. F. Lobdell, "Impact Response of the Human Thorax," *Proceedings of the Symposium Human Impact Response Measurement and Simulation* (1973) pp. 201–245.
27. G. W. Nyquist, J. M. Cavanaugh, S. J. Goldberg and A. I. King, "Facial Impact Tolerance and Response (SAE Paper No.861896)," *Proceedings of the 30th Stapp Car Crash Conference* (1986) pp.379–400.
28. H. Gray, *Anatomy of the Human Body* (Lea & Febiger, Philadelphia, 1918).
29. J. Horsch and D. Schneider, "Biofidelity of the Hybrid III Thorax in High-Velocity Frontal Impact," SAE Paper No.880718. (1988).
30. FMVS Standards, *FMVSS 208 - Occupant Crash Protection* (2004).

Jung-Jun Park received the B.S., M.S. and Ph.D. in Mechanical Engineering from the Korea University in 2000, 2005 and 2010, respectively. His current research interests lie mainly in a safe manipulator and safe physical human–robot interaction.

Jae-Bok Song received the B.S. and M.S. degrees in Mechanical Engineering from Seoul National University in 1983 and 1985, respectively, and the Ph. D. degree in Mechanical Engineering from MIT in 1992. He joined the faculty of the School of Mechanical Engineering, Korea University in 1993. Currently, he is a director of Intelligent Robotics Research Center at Korea University. He is also an Editor-in-Chief for International Journal of Control, Automation and Systems. His current research interests include safe manipulators, design and control of robotic systems, and mobile robot navigation.

Sami Haddadin received his Dipl.-Ing. degree in Electrical Engineering in 2006 from Technical University of Munich and holds an Honours degree in Technology Management from Technical University of Munich and the Ludwig Maximilian University Munich. He obtained the Ph. D. degree from RWTH Aachen. He currently works at Institute of Automatic Control, Leibniz University Hanover (LUH) as a Director. His main research topics are physical Human–Robot Interaction, robot control, and safety and dependability in robotics.